



HAL
open science

In Situ Spectroscopic Imaging of Devices for Electrochemical Storage and focus on the solid components

Elodie Salager

► **To cite this version:**

Elodie Salager. In Situ Spectroscopic Imaging of Devices for Electrochemical Storage and focus on the solid components. Sabina Haber-Pohlmeier; Bernhard Blumich; Luisa Ciobanu. Magnetic Resonance Microscopy: Instrumentation and Applications in Engineering, Life Science, and Energy Research, wiley, 2022, 978-3-527-82725-1. 10.1002/9783527827244.ch16 . hal-03856821

HAL Id: hal-03856821

<https://hal.science/hal-03856821>

Submitted on 17 Nov 2022

HAL is a multi-disciplinary open access archive for the deposit and dissemination of scientific research documents, whether they are published or not. The documents may come from teaching and research institutions in France or abroad, or from public or private research centers.

L'archive ouverte pluridisciplinaire **HAL**, est destinée au dépôt et à la diffusion de documents scientifiques de niveau recherche, publiés ou non, émanant des établissements d'enseignement et de recherche français ou étrangers, des laboratoires publics ou privés.



Distributed under a Creative Commons Attribution - NonCommercial - ShareAlike 4.0 International License

16. In Situ Spectroscopic Imaging of Devices for Electrochemical Storage and focus on the solid components

Elodie Salager

CNRS, CEMHTI UPR3079, Université d'Orléans, Orléans, France

Réseau sur le Stockage Electrochimique de l'Energie (RS2E), CNRS FR3459, Amiens, France

16.1 Introduction

Energy storage becomes increasingly crucial in the transition from fossil energy to renewable energies, which are intrinsically intermittent. Electrochemical storage is one of the currently exploited answers and received a lot of attention already. The corresponding devices, mainly lithium-ion batteries (LiB) and electrochemical double layer capacitors (EDLC), are omnipresent in today's life. Mobile applications range from small portable electronics to electrified transport, and stationary storage is increasingly important.

The ultimate goal is to obtain devices with high power (fast charge or delivery of energy), high capacity (autonomy) and long lifetime. Power and capacity are difficult to optimize jointly, so that the emphasis is put on one or the other characteristics depending on the intended use.

While a full understanding of the mechanisms of storage is essential to devise new materials for enhanced energy storage and power, the parasitic chemical reactions or morphological evolutions undergone on the longer-term (after multiple cycles) often relate to capacity loss and therefore device lifetime. In addition the LiB and EDLC energy-storing materials are highly reactive and prompt to metastable (electro)chemical states. Unsurprisingly there is a strong demand for characterization techniques that can follow in real time their global evolution and ideally the evolution of each of their components, as demonstrated by several reviews on that subject [1–3].

Magnetic resonance microscopy (MRM), usually defined as magnetic resonance imaging (MRI) techniques with resolution below approximately 100 μm [4], fits in the limits of the spatial requirements for these devices. Its relatively low sensitivity

compared to other techniques is counterbalanced by its non-ionizing characteristics and the low deposited energy that does not degrade the highly reactive constituents.

In this chapter we concentrate on *in situ* Magnetic Resonance (MR) spectroscopic microscopy of the contents of fully functional electrochemical storage devices, for which a complete NMR spectrum is correlated to a specific voxel in the image. The heterogeneity and complexity of the electrochemical devices, however, call for using more constraints than just the spin density to interpret the images obtained during operation. The spectroscopic information is an asset for such studies, thanks to the strong sensitivity of the NMR spectrum to the chemical environment. The resulting spectroscopic images can also be regarded as localized spectra. The goal of this chapter is not to review exhaustively the *in situ* MR field for electrochemical storage, as a number of reviews were published in the recent years.[5–10]. Instead, we introduce, using selected examples, the specific challenges for *in situ* and *operando* MR of electrochemical devices and highlight for solids the opportunities offered by the full exploitation of the combination of the two MR modalities: spectroscopy and imaging.

16.2 Electrochemical Storage

This part aims at giving a rapid overview of the electrochemical storage devices. Further details are available in reference books [11–14].

16.2.1 Li-ion Batteries

Lithium-ion batteries (LiB) rely on reversible reduction-oxidation (redox) electrochemical reactions occurring in the two electrodes to store and deliver energy [15,16]. On discharge, the reduction at the positive electrode captures electrons that are released by the oxidation at the negative electrode. Those electrons are exchanged through the load (phone, computer, car...) and provide current to it. On charge, the charger provides energy to the battery to perform the inverse redox reactions (Figure 16.1a). In commercial Lithium-ion batteries these reactions are associated with reversible intercalation of lithium ions (i.e. without major change the structure) in the active material, hence their name.

Commercial Li-ion batteries use layered transition metal oxides as the positive electrode, such as NMC (for $\text{Li}(\text{Ni}_y\text{Mn}_z\text{Co}_{1-y-z})\text{O}_2$) or Li-rich NMC (with extra Li ions in the transition metal sites).[17] Graphite is classically used as a negative electrode, with the possibilities of silicon-graphite blends being extensively explored [18,19]. The electrodes are electrically insulated by a porous separator; and the electrolyte - usually a salt dissolved in carbonate solvents with various additives – soaks the separator and the electrodes. The requirements for transport electrification have triggered a large body of work to enhance the existing technology, in terms of capacity (amount of stored energy per charge), power (rate of charge), coulombic efficiency (longer lifetime of the battery) and sustainability, but there are still fundamental challenges to meet to cover a larger range of applications [20–22].

Lately a significant effort was made to replace the liquid carbonate solvent -flammable- with a solid electrolyte. The main issues are the lower conductivity and chemical reactivity with the electrodes.[23] Other technologies including Na, K and multivalent ions are also enthusiastically explored in post-Li-ion or all-solid-state batteries.[24,25]

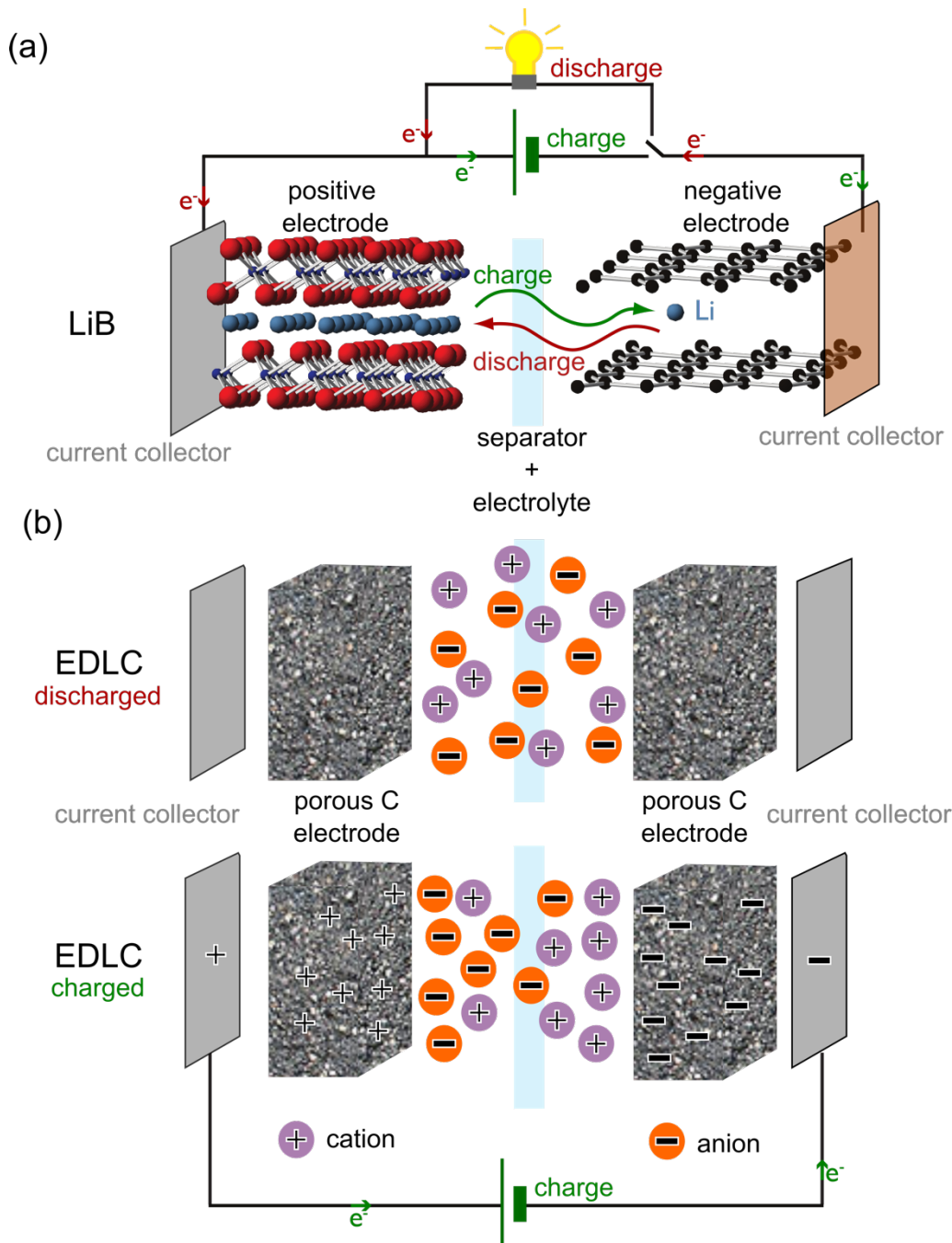


Figure 16.1 Schematics of LiB and EDLC electrochemical mechanisms. (a) The LiB concept relies on redox reactions: exchange of electrons through the electrical circuit and exchange of Li ions through the separator. (b) The EDLC is based on the capacitive behaviour of each electrode-electrolyte interface. The capacitance is obtained through accumulation of charges in the nanoporous carbon electrodes and organization of the ions in the electrolyte. Energy is released through the load, which permits the exchange of charges.

16.2.2 Electrical Double Layer Capacitors

Electrical double layer capacitors (EDLC) correspond to a different usage, with smaller autonomy but high power (fast delivery of energy). In EDLC energy is not stored through faradic processes but through capacitive mechanisms [26]: the electronic charge accumulates on the electrodes and it is charge-compensated by the organization of the ions in the liquid electrolyte (formation of a double layer) and adsorption on the surface of the electrodes (Figure 16.1b). The most common electrodes are nanoporous carbons with controlled porosity. The electrolyte is usually a salt in an organic solvent to enlarge the voltage range and hence the capacitance. The capacitive nature of the energy storage process allows for faster energy storage and delivery (higher power) than in Li-ion batteries, but the stored charge is lower. EDLC have however met a large range of applications, in which power and light weight are strong requirements while an autonomy of minutes is acceptable. The challenge relies on storing more energy, though carefully-designed electrolytes and fine control of the electrode-electrolyte interface, or using hybrid devices such as pseudo-capacitors and Li-ion capacitors [27–29,26,30].

16.2.3 Electrochemical characterization

A large range of electrochemical characterizations is available for LiB and EDLC [31,32]. The electrochemical performance of new electrode composites, electrolyte compositions or chemistries is usually characterized first through multiple charge-discharge cycles. In practice a galvano-potentiostat controls precisely the current or the voltage applied to the battery or EDLC and measures the cell voltage or current response, respectively. Experimentally, a cable links the galvano-potentiostat (and its electronics) to the electrochemical device, using small BNC or clip terminations. Frequency-dependent impedance measurements also provide information on the limiting factors for the electrochemical device.

For batteries, the capacity (amount of charge stored during charge, and returned during discharge) is a key parameter of the electrochemical characterization, as well as the coulombic efficiency (efficiency of the charge-discharge process). Batteries are therefore usually charged and discharged in a galvanostatic mode.

EDLC's stored energy and power depend on the maximum allowed voltage, on the accessible surface area of the electrode and on the average distance between the

adsorbed ions and the electrode surface. Cyclic voltammetry is the common characterization tool for EDLC; the current is ramped between 0 V and the maximum allowed by the electrolyte and returned to its initial value.

Two electrochemical procedures are also relatively common, and especially interesting for *in situ* studies, as they correspond to longer times and allow for (pseudo)equilibrium of the device. In the first procedure - open circuit (OC) - no current is applied to mimic resting stages. The voltage may be followed to determine its equilibrium value and the time needed to reach it. This process is also applied in the Galvanostatic or Potentiostatic Intermittent Titration Technique (GITT or PITT) to determine the kinetic overpotentials and equilibrium potentials in galvanic cells [33,31]. The second procedure, often termed “constant-voltage” (CV) or “floating”, maintains the voltage at a chosen value to characterize the decreasing current. In EDLC this allows stabilizing the electrode/electrolyte potentials and is sometimes used as a way to mimic aging due to multiple cycles of charge-discharge [27].

16.2.4 Electrochemical Device in Practice

The Li-ion battery or supercapacitor is a multi-component device [15] as shown in Figure 16.2, including:

- an airtight casing (stainless steel for cylindrical and coin cells, aluminized plastics for prismatic or pouch cells) with electrical contacts to enable charge and discharge
- a positive electrode and a negative electrode
- an electrolyte, electronically insulating but ionically conducting

The electronic insulation is provided in the case of liquid electrolytes by a microporous membrane (separator), porous to ions to ensure ionic conduction.

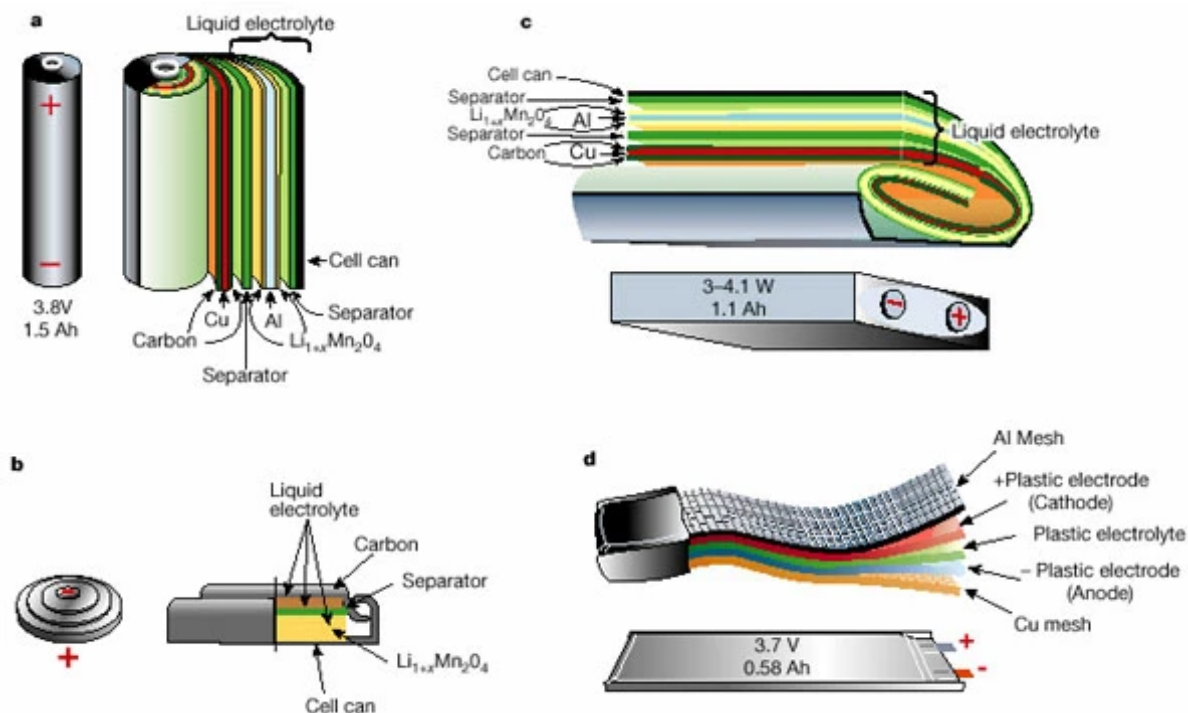


Figure 16.2 Lithium-ion battery devices. (a) cylindrical cell, (b) coin cell, (c) prismatic cell and (d) pouch cell. Reproduced with permission from [15].

The electrodes contain each the electrochemically active material (redox or double-layer), a binder for mechanical strength and processability, and a conductive additive for better electronic conductivity. Note that, contrary to LiB, standard EDLC contain similar positive and negative electrodes.

16.3 Opportunities and Challenges for *In Situ* Magnetic Resonance Spectroscopic Imaging of Electrochemical Storage Devices

Let us first define three terms used in this chapter: *ex situ*, *in situ* and *operando*. This specific terminology was developed to discriminate three different ways of approaching the characterization of an electrochemical device. *In situ* originates from Latin and means “in the natural, original, or appropriate position” [34]. In our case, an *in situ* measurement is performed on the fully operational device – but not necessarily functioning during the measurement. *Operando*, Latin for “operating”, is a subgroup of *in situ* studies and was devised to indicate the characterization of the electrochemical cell while it is operating, i.e. while it has current flowing through. Both terms are commonly opposed to *ex situ*, used for “out of the natural position” and referring to studies for which the components are extracted from the electrochemical cell, thereby destroying the device at each state of charge of interest.

16.3.1 General experimental setup

The experimental setup includes the elements necessary for the MR measurement – supraconducting magnet, magnetic field gradient, RF-resonator and the circuit to the corresponding electronics (pulse programmer, transmitter, RF amplifiers, receiver, digitizer, *etc.*) [35,36], but also the electrical circuit to connect the electrochemical cell to the galvano-potentiostat (Figure 16.3).

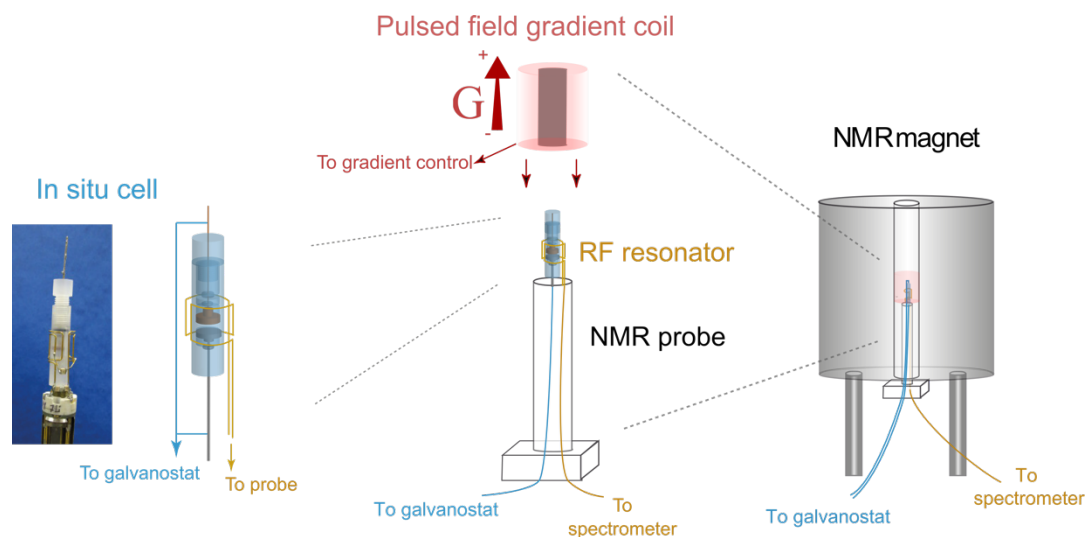


Figure 16.3 General experimental setup of *in situ* MR experiment. Electrochemical cell and probe designs for MR spectroscopic imaging are presented in section 16.4.

16.3.2 Opportunities

The highly heterogeneous nature of the electrochemical devices results in a complex overall MR signal. The wide range of constitutive materials in the device (metals, paramagnetic oxides, conductive powders, liquids, microporous separator membranes...) results in distortions of the *in situ* MR images that are difficult to identify. Strongly-shifted peaks may also create artifacts in the images and magnetic susceptibility blurring at the interfaces are common issues.

Reversing the approach and looking at it as *in situ* MR spectroscopist, assignment of the peaks in the MR spectrum to the various components of the battery is essential to extract relevant information about its evolution. This is challenging due to the numerous interfaces at the microscopic scale that result in shifts and broadenings (mainly magnetic susceptibility effects [37,38]).

But this complexity is also an opportunity, as it contains precious information about the contents of the device. The combination of the spectroscopic and spatial dimensions

enables an easier exploitation of that information. Figure 16.4a shows the spectrum of a Li-ion battery containing a paramagnetic positive electrode (not detected), a negative lithium electrode and a standard electrolyte, LiPF₆ in EC:DMC (1:1). The signal for the electrolyte spans the zone -5 ppm to 15 ppm, a range ten times larger than the ⁷Li chemical shift range for diamagnetic compounds. In this case the chemical information is negligible compared to other effects in the cell. In Figure 16.4b and c, localization adds an extra dimension to expand the spectrum in and helps assigning efficiently the spectra. The negative shifts can be assigned to electrolyte out of the electrochemical core, above the copper and below the aluminium current collectors.

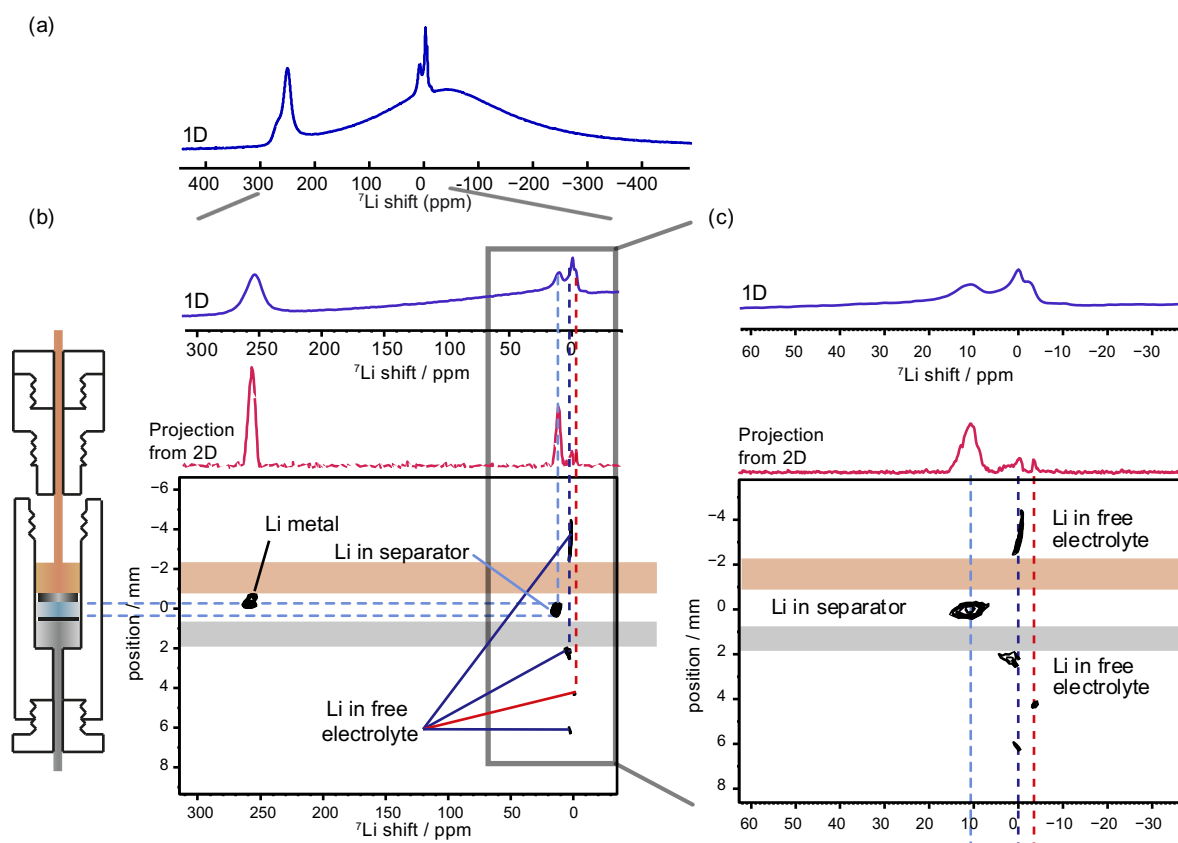


Figure 16.4 *In situ* ⁷Li MR data of a Li₂Ru_{0.75}Sn_{0.25}O₃/Li battery with LP30 electrolyte (a) spectrum (b) chemical shift 1D image and (c) close up on the electrolyte part. Adapted with permission from [39]. Copyright (2014) American Chemical Society.

The spectroscopic information is often reduced to the chemical shift, considered as the most relevant spectroscopic information thanks to its sensitivity to the chemical environment. The NMR spectrum provides in reality more than just the shift to the

image. Several other characteristics (width, shape, relaxation, diffusion, connectivity maps) can be correlated to each peak and their evolution followed as the device is charged and discharged. These characteristics are also critical to exploit and correct distorted images.

In short, *operando* spectroscopic imaging or localized spectroscopy is a multi-dimensional measurement, in which the image dimension can be in principle either 1D (profile), 2D (slice or projection) or 3D, while the spectroscopic information for each slice/pixel/voxel is in the form of a 1D spectrum, or a series of 1D spectra used to extract other parameters such as relaxation times (T_1 , T_2 , T_2^*), self-diffusion coefficients, or even n-dimensional spectra.

An important feature of *operando* or stop-and-go *in situ* measurements is the evolution of the contents of the electrochemical device upon charge and discharge, as it stores and releases energy. Following the *evolution* of the device brings time as an additional dimension, which is useful to analyze and discriminate components compared to a single spectroscopic image. A last group of dimensions is therefore formed by the electrochemical properties (state-of-charge, impedance, galvanostatic or potentiostatic intermittent titration...).

The only limit to dimensionality is the time required to record data with a satisfying signal-to-noise ratio.

16.3.3 Experimental Challenges

The first *in situ* measurements were performed using a home-made design with a toroid cavity, with a Cu foil having a dual functionality: current collector and NMR detector [40]. In these pioneering study, rotating frame NMR imaging was used to obtain the spectra as a function of distance from the centre of a radial cell and detect lithium plating on a carbon electrode. This approach however prevented *operando* measurement, as no charging current could flow in the detector during the measurements.

Innovative strategies are currently explored by Jerschow and coworkers, with the aim of keeping the commercial aluminium casing. In a first step, the commercial electrochemical device was studied without any modification, using pure MRI. The state of the device was observed indirectly by distortions in the image of a liquid filling a surrounding reservoir [41–43]. This original approach allowed for fast screening of

defective cells, with measurement times as small as 12 s for a two-dimensional image. Spectroscopy was not possible however, so that the chemical origins of cell failure cannot be tracked. Instead, the cell image was compared to a pre-made database of functional and dysfunctional cells to identify the source of failure. Key features were identified using statistical tools, such as principal components analysis (PCA). Another creative approach has been to use the casing of the device as the resonator, and promising NMR spectra of the inside of an aluminized battery pouch cell were obtained [44]. This second approach did not provide spectroscopic imaging data yet.

The most popular approach, which was used for MR spectroscopic imaging, was pioneered by Letellier *et al.* in 2003 for Li-ion batteries [45] and fully exploited by Grey *et al.* [5]. The principle is to separate physically the electrochemical and MR circuits. One of the key advantages of that approach is to enable *operando* measurements, *i.e.* with current flowing in the cell during the MR measurement. Additionally the device can be transferred from or to an electrochemical bench for preliminary or additional charge and discharge.

Two main practical challenges are faced for *in situ* MR of electrochemical devices. The first challenge comes from the electrical circuit running between the galvanopotentiostat and the device, through the MR magnet and RF resonator. Coupling to the RF resonator brings parasitic signals that alter significantly the signal-to-noise ratio of the MR experiment, even without current running. A careful choice of shielded electrical cables and low-pass filters (cutoff frequency well below the Larmor frequency of the nuclei of interest) efficiently reduce the noise pickup at the Larmor frequency and restores a better signal to noise ratio.

The second challenge is the low penetration of the radio-frequency (RF) field through conductors: less than 10 μm in aluminium for a RF carrier frequency of 77 MHz, corresponding to ^7Li in a 4.7 T magnet. Stainless steel and aluminized casings shield the contents of the device from orthogonal time-dependent RF fields, inducing eddy currents and blind zones near the current collectors [46]. Letellier's approach and its derivatives are associated with the design of a specific geometry for the electrochemical cell to prevent issues in RF shielding from the cell, keeping the probe largely unmodified - apart from the RF resonator in some cases. These designs are described further in section 16.4.

16.3.4 Quantitative measurements

Another issue, often neglected, is the difficulty of performing properly quantitative measurements. These are challenging as several factors act on the signal intensity, with varying strength as the device is charged and discharged. First, part of the signal may be broadened beyond detection for some states of charge, changing the total intensity of the spectrum. Changes in the conductivity or the charge of the constituents modify the quality factor of the measuring circuit (hence the overall intensity of the spectrum). The NMR relaxation properties also vary with the state-of-charge and must be determined prior to the *operando* measurement or on the fly, resulting in a loss of time resolution. The last issue is the limited penetration of the RF wave in the bulk of metallic conductors, which results in a heterogeneous RF field strength distribution and excitation of the spins in the metallic electrodes. Metallic transitions upon lithiation or delithiation are relatively common in positive and negative electrodes (e.g. LiCoO₂, graphite). Concentration profiles were however obtained through analysis of spectroscopic images [47–49].

16.3.5 Time Resolution and Sensitivity

In situ and *operando* MR Imaging of electrochemical storage devices is demanding, especially regarding spatial and temporal resolution: battery components are usually around or less than 100 μm thick and the target for electric car batteries is set to charging in as fast as 15 minutes. Time resolution is an important point to take into account, as the MR measurement is an average of the battery states over the recording time. In particular, spectroscopic imaging measurements are relatively long to record, so that during the course of recording a non-negligible evolution of the state of charge may occur. The device may be left in open-circuit to avoid this “temporal blurring” and the MR data recorded only after stabilization of the electrochemical state – this “stop-and-go” *in situ* approach is not strictly *operando* but provides relevant snapshots of the battery state without opening it.

Space and time resolution are ultimately limited by sensitivity. As a result, *in situ* MR spectroscopic imaging is usually limited to sensitive isotopes, such as ¹H, ¹⁹F, ³¹P, ⁷Li. For the solid components, the dimensionality is limited to spectroscopic 1D profiles or slice-selective measurements, using a compatible electrochemical cell geometry.

16.4 Electrochemical Cells and Probes designs for *In Situ* Spectroscopic Imaging

Performance of the MR spectroscopic imaging is intimately linked to the probe design: PFG strength and match between the sample holder and the RF resonator. Electrochemical cell and probe designs have been explored enthusiastically to increase sensitivity.

Most of the work performed for *in situ* MR spectroscopic imaging follows Letellier's pouch cell approach, with variations in the design and geometry of the dedicated electrochemical cell. Three main families of setup have been successfully used to study Li-ion batteries and supercapacitors: pouch cells, Swagelok cells and plastic capsule cells (Figure 16.5). Improvement of the designs is still on-going work and numerous variations in each design have been published; in the following only the electrochemical cells that were used for spectroscopic imaging are reported, with reference to the seminal work of the corresponding design.

Commercial micro-imaging probes with 3D-PFG, or probes meant for diffusion measurements (1D-PFG), are commonly employed. The 3D-PFG are relatively moderate (up to $3 \text{ T}\cdot\text{m}^{-1}$) while in the 1D-PFG design a stronger pulsed-field gradient is available ($30 \text{ T}\cdot\text{m}^{-1}$) by sacrificing the two other directions.

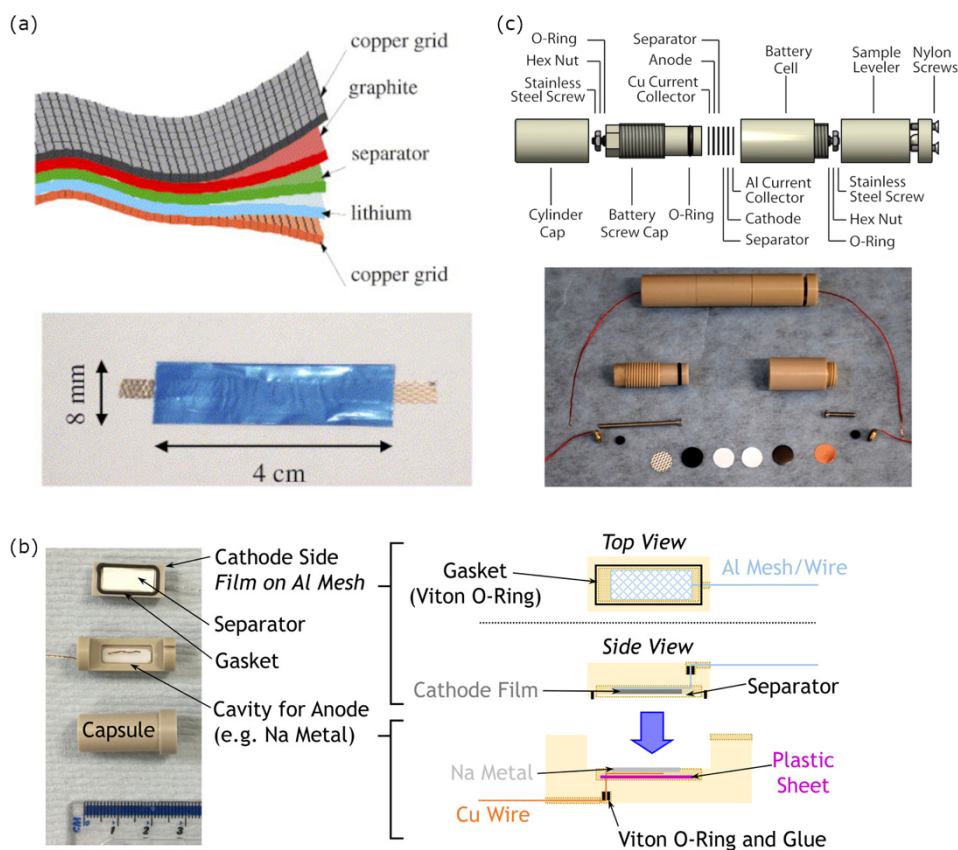


Figure 16.5 Electrochemical cells for *in situ* MR (a) pouch, (b) capsule and (c) Swagelok. Reproduced with permission from [50–52] respectively.

16.4.1 Pouch Cells

The first pouch cells for *in situ* NMR spectroscopy had an aluminized blue plastic film sealed as a pouch around the battery. The electrode and separator films were plasticized and laminated onto copper grids that came out of the pouch (Bellcore technology [53,54], Figure 16.5a).

Chandrashekar et al. were the first to use this design in 2012 for *in situ* chemical shift-2D imaging on symmetric Li//Li cells [55] placed in an NMR tube. They used a simple polyester film as the casing; the removal of the aluminium barrier lowered the gas-tightness of the casing but enhanced the MR sensitivity. Lithium dendrite formation could be characterized *in situ*, using the chemical shift information to discriminate bulk metallic lithium from mossy and dendritic lithium.

16.4.2 Plastic Capsule/Cartridge Cells

A plastic “cell capsule” was designed in Grey and Jerschow groups [51] (Figure 16.5b). This design uses rectangular electrodes sitting between two polyetheretherketone (PEEK) half-cylinders. Air-tightness is ensured by compression of a rectangular sealing gasket, pressure is provided using chocks that press the electrochemical core inside the casing. The first use of the plastic cell capsule for spectroscopic 2D-imaging was performed by Ilott et al. on supercapacitors in 2014 with a polytetrafluoroethylene (PTFE) cell [56]. It enabled separating the spectroscopic signatures of the ions in the two similar electrodes in *in situ* and *operando* modes.

16.4.3 Swagelok Cells

A cylindrical polypropylene housing (Swagelok design) was pioneered in 2011 by Poli et al. for *in situ* NMR spectroscopy but it was not described precisely [57]. It inspired the development in 2013 by Tang et al. of a PEEK cell for *in situ* stray-field MR imaging (STRAFI), an approach using the strong fringe field of a magnet that unfortunately does not allow for spectroscopic measurements [58,52]. The electrode disks are perpendicular to the cylinder axis and sandwich a separator soaked with liquid electrolyte, with several O-rings ensuring air-tightness. The main advantage of that design compared to the two others is the better control on compression *via* the screw cap (Figure 16.5c). The first report of spectroscopic imaging with this family of cells was shortly afterwards by Salager *et al.* [39]. Their cell was machined in polychlorotrifluoroethylene (PCTFE), a transparent plastic enabling easier positioning of the battery’s electrochemical core in the probe. In this study *in situ* chemical shift-1D imaging enabled the localization of the signals for the electrolyte and metallic lithium, including those distorted by the conductors in the electrochemical cells.

16.4.4 Promising designs

A promising design from Balcolm and coworkers was recently published. This cartridge design, close to the pouch cell geometry [59], made of plastic (garolite/PC board) plates and sealed by compressing a silicon rubber gasket with screws running through the plastics. This cartridge is inserted in a parallel plate resonator within a home-made probe, using commercial PFG (max 0.3 T.m⁻¹). ⁷Li T₁-T₂ correlations identified the electrolyte located in different environments (separator, electrode

porosity) and in the graphite electrode. Up to now only T_1 - T_2 maps were published, without further spectroscopic information, owing to the low homogeneity (1 ppm) and intensity of the magnetic field used in the study (2.4 T).

Another promising design, similar to a jelly roll, was proposed by Freytag et al. [60,61]. The current collectors were replaced by cellulosic paper and allowed charging the battery very slowly (one charge in 100 hours). The RF penetration is optimum and the cell could be spun in the magnetic field, resulting in better spectral resolution. The design still needs improvement, as lithium dendrites should not form at such low charging rates, but the concept may enable spectroscopic imaging using rotating PFG synchronized with magic angle spinning [62].

16.5 Classical chemical shift imaging for the solid parts of batteries

The electrochemical device components are extremely heterogeneous in terms of NMR characteristics: the liquid electrolyte, narrow with long signal lifetime; and the solid components, broad and usually short signal lifetime. The field of pure MR imaging has been rapidly expanded to image the solid components of a battery, using for example spin or gradient echoes for the narrowest signals (mobile electrolyte) and Single Point Imaging (SPI) and derivatives [8–10,63–65] for the broader signals (solid electrodes).

16.5.1 Signal lifetime

The spectroscopic imaging approach is usually optimized for a given component of the battery. A constraint for chemical shift imaging (CSI) is that the signal lifetime of the material under study must be longer than the manipulation of magnetization for the chemical shift image formation.

The initial studies with *in situ* CSI focused on the liquid electrolyte, thanks to better sensitivity. Indeed, the liquids in the EDLC or battery are the easiest to record, mainly due to their narrow peaks, high intensity and long lifetime. Chemical shift imaging of the electroactive ions (detected with ^{11}B and ^1H) provided atom-specific information, localized at the positive or the negative electrode [56]. CSI was also performed to correct 1D profiles for the study of polarization in liquid electrolytes at various temperatures [48]. Dynamics (diffusion and relaxation) is also the subject of active research: recent examples of slice-selective self-diffusion coefficients or slice-

selective relaxation measurements applied to the liquid electrolyte of batteries can be found in Refs. [47,49,66,67]. Solids have faster transversal relaxation, so that the duration of the spin echo must be shortened considerably, as will be discussed in the following.

16.5.2 Phase-encoded Chemical Shift 1D Imaging sequence

A classical phase-encoded sequence used for MR spectroscopic 1D imaging is displayed in Figure 16.6.

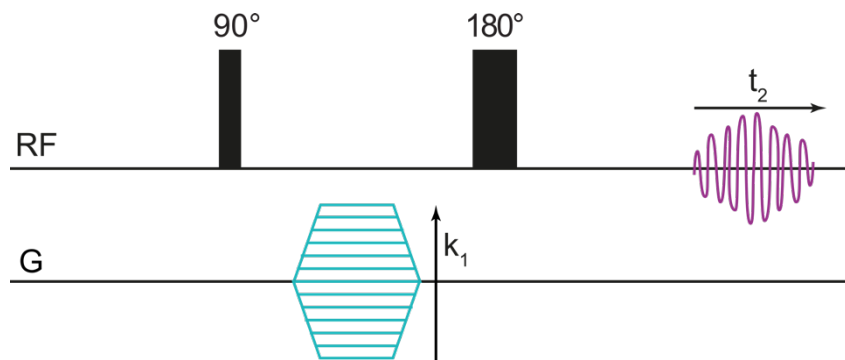


Figure 16.6 Chemical shift 1D imaging sequence. A Hahn-echo is performed with a PFG in the first evolution period (in cyan) to phase-encode position. The spatial dimension is encoded as a phase evolution, obtained from the incrementation of the PFG strength for each new slice.

This version of Chemical Shift Imaging (CSI) [68] is based on a spin echo, with the free induction decay recorded in the direct dimension. The spatial dimension is encoded as a phase evolution in the first half of the echo, obtained by applying a pulsed field gradient (PFG). The PFG amplitude is ramped at every increment in the indirect dimension to sample the reciprocal space:

$$G_n = \frac{n}{L} G_{max} \quad \text{Equation (16.1),}$$

with n varying in $2L$ steps from $-L$ to $L-1$.

The spatial dimension is recovered by Fourier Transform against the reciprocal space vector k_n , defined as:

$$k_n = \frac{1}{2\pi} \int_{t=0}^{t_p} \gamma G_n f_G(t) dt \quad \text{Equation (16.2),}$$

with t_p the PFG pulse duration, γ the gyromagnetic ratio, $f_G(t)$ the normalized temporal shape of the PFG pulse.

In the case of a perfect rectangular gradient pulse, $f_G(t)=1$, and

$$k_n = \frac{1}{2\pi} \gamma G_n t_p \quad \text{Equation (16.3).}$$

The field of view (*FOV*) is then given by :

$$FOV = \frac{1}{\Delta k} = \frac{2\pi}{\gamma \Delta G t_p} \quad \text{Equation (16.4),}$$

with Δk the increment in reciprocal space vector, ΔG the increment in the gradient amplitude.

Replacing ΔG with G_{\max}/L in Equation (16.4) results in:

$$FOV = \frac{2\pi L}{\gamma G_{\max} t_p} \quad \text{Equation (16.5).}$$

The slice thickness is controlled by the gradient duration and maximum amplitude:

$$S = \frac{FOV}{2L} = \frac{\pi}{\gamma G_{\max} t_p} \quad \text{Equation (16.6).}$$

A smaller slice thickness can be obtained by an increase in G_{\max} , but in order to keep the FOV identical it must be compensated by an increase in the number of encoding steps L . Better resolution therefore requires longer recording times: more encoding steps are needed and sensitivity is lowered due to the smaller number of atoms within each slice. Sensitivity is again the limiting factor.

16.5.3 Metallic electrode

The signals of metallic electrodes have shorter characteristic lifetimes, but classical chemical shift imaging techniques can still be applied provided that short echo times are used - the PFG strength is increased to shorten the PFG pulse duration and keep reasonably small slice thickness. Note that the FOV may be distorted for extremely short delays by non-ideal PFG shapes and eddy currents from the last RF pulse.

The peak positions are shifted from the diamagnetic parts (Knight shift), making them easier to identify in the spectrum and reducing the need for imaging. Small variations in morphology impact slightly the shift [69], so that chemical shift imaging can be useful to localize newly formed dendrites or mossy structures.

Although the Knight-shifted signal of metallic lithium is easily separated spectrally from the other constituents, it has been a great playground for *in situ* MR studies, thanks to its reasonable transversal relaxation and sensitivity of the shift to morphology.

Chandrashekar et al. implemented the first chemical shift imaging measurements on a symmetric Li//Li cell in a seminal paper [55]. They demonstrated indisputably that the deposited mossy/dendritic metallic lithium had a slightly different shift compared to bulk lithium. Such assignment had been proposed in a previous *in situ* MR spectroscopic-only study [70].

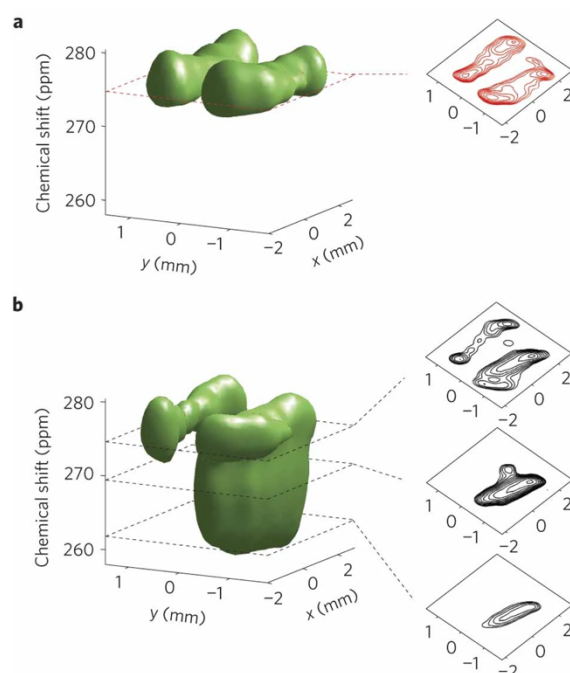


Figure 16.7 CSI of the metallic Li resonance in the pristine (a) and after polarization (b). The two flat electrodes are parallel to the xz plane. In (b), dendritic lithium is evidenced by the signal in the 260-275 ppm range, lower than the Knight shift of the bulk electrode. Reproduced with permission from [55].

Later Chang *et al.* [71] performed CSI in a Li//Li symmetric cell with widely spaced electrodes (flooded cell) to discriminate the signals of the two electrodes and identify various types of lithium microstructures from their shift. Their formation could be linked with lithium depletion in the electrolyte near the lithiating electrode in fast charging mode, thanks to *in situ* 1D profile of the electrolyte in the cell. Importantly, this study demonstrated experimentally the validity of Sand's model in that case (Figure 16.8).

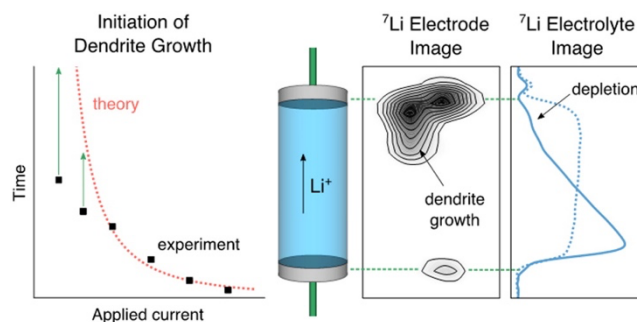


Figure 16.8 Plot showing the time (capacity) at the onset of dendritic growth (black squares) and Sand's model for simulating the evolution (red line). Center: electrochemical flooded cell, right, CSI of metallic Li and 1D profile of the electrolyte. Adapted with permission from [71]. Copyright (2015) American Chemical Society.

Metallic Sodium does not necessitate chemical shift imaging as the shift of metallic Na is so different from that of other Na-containing compounds that they can be discriminated by using the limited bandwidth of the probe [65,72–74].

16.5.4 Solid electrolyte

In situ Chemical Shift 1D imaging was performed by Marbella et al. [75] to identify dendritic growth in a garnet-type solid electrolyte (LLZTO), promising for all-solid-state lithium-ion batteries. In Figure 16.9c, the ^7Li signal for the electrolyte appears near 0 ppm while additional signal located inside the separator appears at the shift of microstructural Li after polarization. It is ascribed to metallic Li dendrites forming across the solid separator.

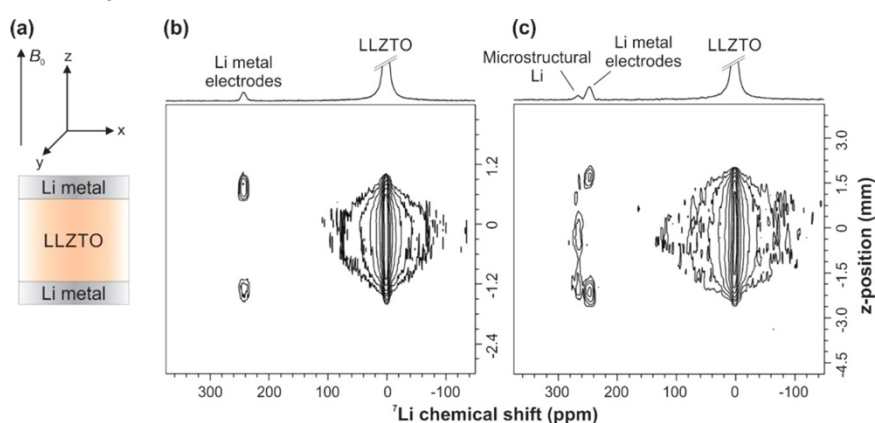


Figure 16.9 (a) Schematic of a symmetrical Li–LLZTO–Li cell depicting the orientation with respect to the external magnetic field, B_0 , during the ^7Li CSI experiment. ^7Li chemical shift images of (b) pristine and (c) cycled Li–LLZTO–Li symmetrical cells. The ^7Li NMR signal of

LLZTO is significantly more intense than that of Li metal and is truncated as indicated by hashes. Reproduced from [75], published under a CC-BY licence.

16.6 A specific sequence for paramagnetic electrodes: S-ISIS

The most difficult part to image in a Li-ion battery is the paramagnetic electrode, containing unpaired electrons localized around the transition metal atoms. Dipolar and Fermi-contact nucleus-electron interaction [76] result in strong shifts and broadenings, so that the typical transverse relaxation times of those solids (T_2') are smaller than 100 μs . Classical chemical shift imaging approaches, based on spin echoes become inefficient: the signal of the paramagnetic electrodes is absent from the chemical shift image (Figure 16.4). The echo time cannot be shortened enough, notably because the strong PFG needed for imaging those solids cannot be switched on faster than 1 ms.

16.6.1 1D-ISIS sequence for localized spectroscopy

Despite these constraints, Tang et al. managed to record *in situ* spectroscopic 1D images of a full battery, based on a frequency-encoding sequence [77]. The spectroscopic signature of all the components inside the battery were obtained, including the two solid paramagnetic electrodes, $\text{Li}_{1-x}\text{CoO}_2$ and $\text{Li}_{4+y}\text{Ti}_5\text{O}_{12}$. This was achieved by combining the strongest 1D-PFG available ($24 \text{ T}\cdot\text{m}^{-1}$) with a carefully-designed pulse sequence for localized spectroscopy (Figure 16.10). This pulse sequence was initially designed for localized spectroscopy in living organism and dubbed Image Selected In vivo Spectroscopy or ISIS [78]. Note that the ISIS approach is compatible with 3D, but the resolution would be small, as the commercial 3-axes PFG are currently limited to $3 \text{ T}\cdot\text{m}^{-1}$, one order of magnitude smaller than the strongest commercial 1-axis PFG ($30 \text{ T}\cdot\text{m}^{-1}$).

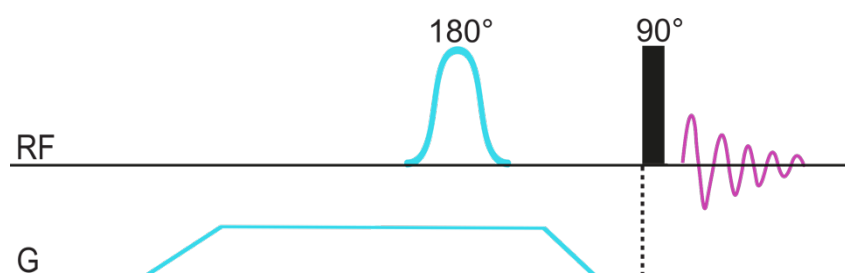


Figure 16.10 ISIS pulse program for 1D localized spectroscopy. Adapted from original work published under a licence CC-BY-4.0 in [77].

First, the PFG is turned on and left to stabilize for at least 1 ms. Then a selective 180° RF pulse inverts the spins in a slice. Finally, the gradient is switched off and the NMR spectrum is acquired. The key point is to switch the PFG off while the spins are experiencing longitudinal relaxation (~ 10 times slower than transversal relaxation). The resulting NMR spectrum contains contributions from both the inverted slice and the non-inverted slices. A reference spectrum is subtracted in order to retrieve the slice spectrum. This reference spectrum is recorded without the inversion pulse (but keeping all delays the same).

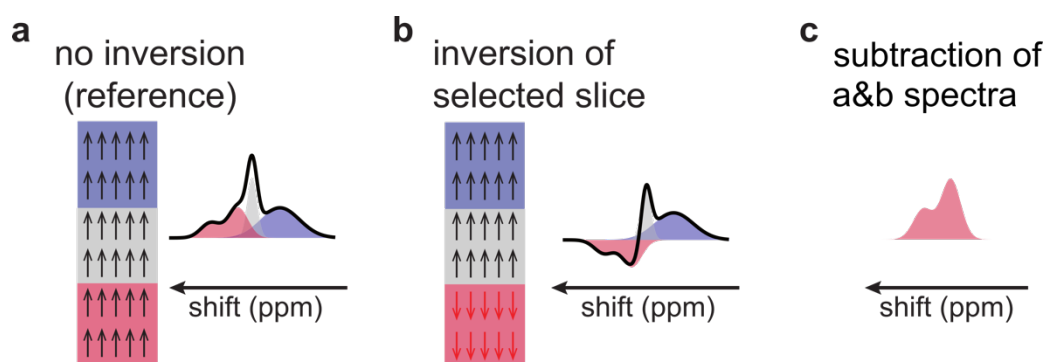


Figure 16.11 Schematic principle of 1D-ISIS using three horizontal slices. (a) The reference spectrum is recorded without the inversion pulse. (b) An inversion, selective for the pink slice, is performed prior to the FID recording. The resulting spectrum contains the contribution of the non-inverted spins in the two other slices and that of the inverted spins in the pink slice. (c) Subtraction of the spectra obtained in (a) and (b) provides the spectrum of the pink slice. Adapted from original work published in [77] under a CC-BY-04 licence.

16.6.2 Slice Selection

The ISIS sequence relies on frequency encoding, as defined in Equation (16.7):

$$\nu(z) = \frac{\gamma}{2\pi} B_0 + \frac{\gamma}{2\pi} zG \quad (16.7),$$

with $\nu(z)$ the frequency of the spins at z distance from the origin of the PFG, γ the gyromagnetic ratio, B_0 the main static magnetic field and G the PFG strength.

The slice centre z is then defined by:

$$z = \frac{2\pi\nu_{pulse}}{\gamma G} - \frac{B_0}{G} \quad (16.8),$$

with ν_{pulse} the RF pulse frequency.

Note that this expression is only valid if the shift from the Larmor frequency due to the other interactions (chemical, paramagnetic, Knight, susceptibility shift...) is negligible compared to the PFG. If not, slightly displaced images are overlapping that result in a degraded spatial selectivity. The strongest PFG strength should therefore be aimed at.

The peak width of a solid is controlled by a mixture of homogeneous and heterogeneous broadenings, as defined by Maricq and Waugh [79]. The minimal width that can be excited is controlled by the intrinsic width [35] – the set of frequencies that cannot be excited separately, even if the selective pulse was infinitely selective. As a consequence, the smallest achievable slice thickness is:

$$\Delta Z = \frac{2\pi\Delta\nu_{intrinsic}}{\gamma G} \quad (16.9),$$

with $\Delta\nu_{intrinsic}$ the intrinsic width of the spectrum.

16.6.3 Scanning ISIS

Tang et al. went one step further and used the ISIS technique in a scanning mode, dubbed S-ISIS [77]. They recorded the ^7Li spectra of all the slices successively so as to reconstruct the full spectroscopic image, as shown in Figure 16.12. The contributions of the two electrodes, overlapping in a single 1D spectrum could be separated and slices in each electrode could be extracted.

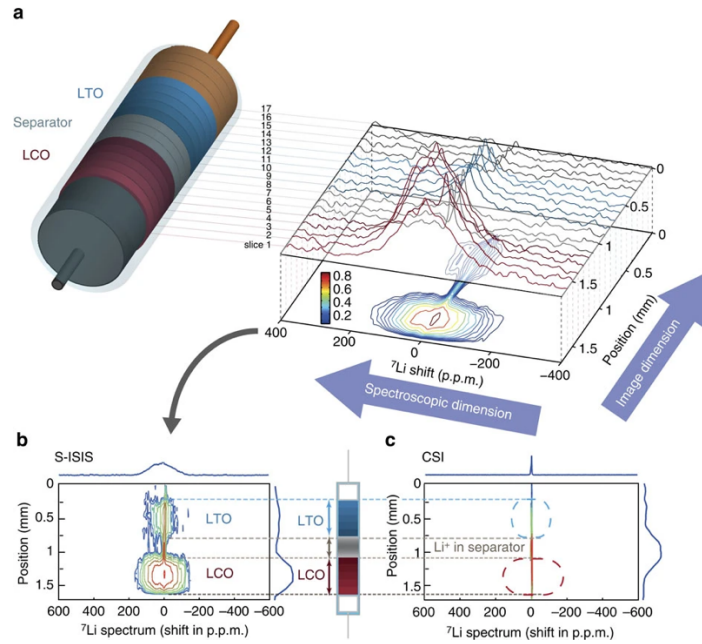


Figure 16.12 ^7Li Scanning ISIS of a $\text{LiCoO}_2/\text{Li}_4\text{Ti}_5\text{O}_{12}$ (LCO/LTO) battery. (a) Series of spectra obtained for horizontal slices of thickness $100\ \mu\text{m}$ in the battery. The spectroscopic image is reconstructed from the series of spectra and correlates spectrum and position. The corresponding contour map is shown below. (b,c) Comparison of the NMR spectroscopic images (contour maps) for the LCO/LTO battery obtained with (b) the S-ISIS method and (c) the standard CSI. Reproduced from [77], published under a CC-BY 4.0 licence.

There is an additional constraint on the slice thickness from the *in situ* measurements. As the device is heterogeneous and contains several materials with variable intrinsic width, the optimal spatial resolution depends on the location in the device. This makes the interpretation intractable unless the localized intrinsic width is measured (*ex situ*) for all states of charge of interest. This option however would reduce time resolution, which is already limited, or it would require analysing destructively tens of batteries per cycle.

In Tang's work the choice was to avoid control by the intrinsic width and ensure the slice thickness is known at all times. The RF pulse bandwidth was chosen so that the intrinsic width of the peaks was negligible compared to it - the slice thickness did not depend any more on the intrinsic width of the spectrum, but only on the RF pulse bandwidth:

$$\Delta Z = \frac{2\pi\Delta\nu_{pulse}}{\gamma G} \quad (16.10),$$

with $\Delta\nu_{pulse}$ the RF pulse bandwidth.

Experimentally, this RF pulse bandwidth was set larger than the largest homogeneous width (38 kHz) obtained in all the materials throughout the battery charge and discharge cycles. The PFG strength was set to the maximum available: $24 \text{ T}\cdot\text{m}^{-1}$ to ensure a spatial resolution of $100 \mu\text{m}$, well controlled over the whole course of the *in situ* study, but worse than what could have been obtained at other states of charge.

16.6.4 S-ISIS study of lithiation fronts in the solid electrodes of the battery

A direct application of this 1D-S-ISIS sequence is the analysis of thick electrodes. Such electrodes are studied for the increase in capacity and hence autonomy, but they usually suffer from kinetic limitations. Visualizing and analyzing the lithiation fronts inside the electrodes provides useful information to identify the origin of the limitations. The redox reaction requires indeed a triple point, where the electrons, lithium ions and transition metal ions must be present. Sluggish kinetics can be due to low percolation of lithium, or electrons, in the material. By construction of the cell, electrons are provided from the current collector side, while lithium ions originate from the electrolyte. The spatial distribution of states-of-charge obtained with 1D-S-ISIS for a given capacity indicates limitation from the electrolyte side, with a slow percolation of the lithium ions inside the electrode bulk.

16.7 EPR spectroscopic imaging for electrochemical storage

Spectroscopic imaging has also been applied in the sister field of Electron Paramagnetic Resonance. At room temperature, magnetic field gradients cannot be pulsed fast enough, so that EPR Imaging is performed by raster ray encoding [80–82]. Recently, Dutoit et al. published an application of spectroscopic imaging to characterize the morphology of lithium particules in a Li//Li battery [83]. The comparison of the 2D images and the 1D-spectroscopic images identifies and locates sub-micrometric particles deposited on or stripped from the metallic Li electrodes during positive and negative polarization, respectively.

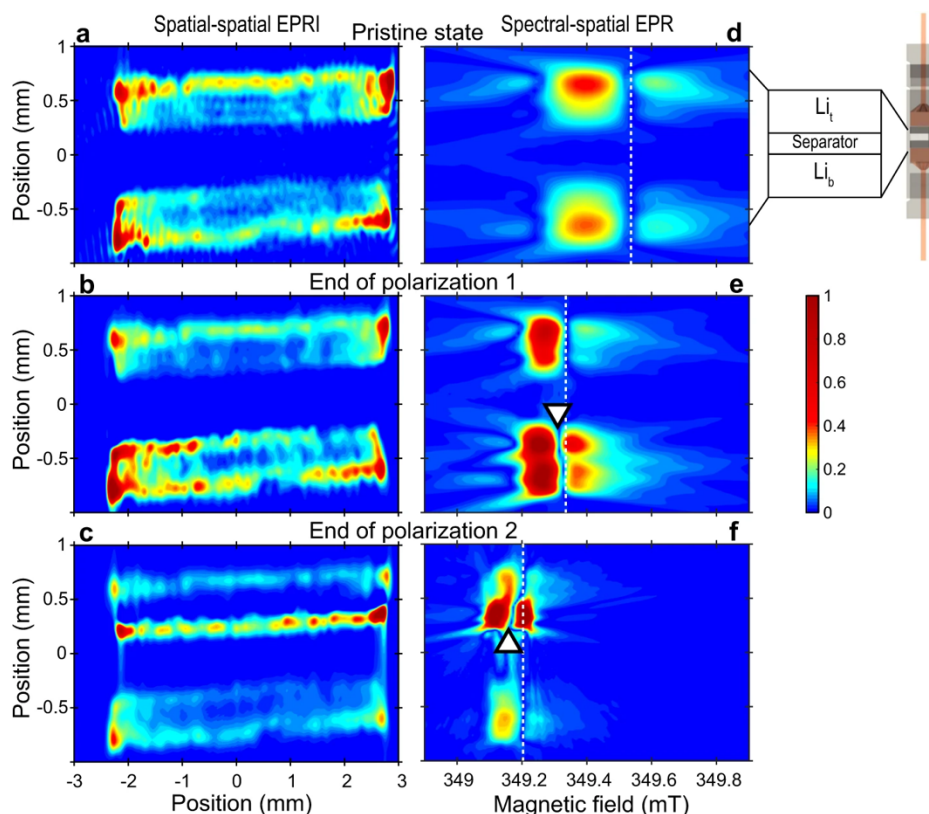


Figure 16.13 2D X-band EPR images of a Li//Li electrochemical cell (a-c) 2D images; (d-f) “spectral-spatial” EPR images between 1D profile and spectrum. Reproduced from [83], published under a CC-BY 4.0 licence.

16.8 Conclusion

Since the first “modern” characterization by *in situ* magnetic resonance spectroscopy of a lithium-ion battery in 2003, the field of *in situ* magnetic resonance of electrochemical devices has expanded to various probe and electrochemical cell designs. MR microscopy has been included into the MR toolbox to obtain localized information. When required, for example when the signals arising from several components of interest in the electrochemical device overlap, correlation of spatial and spectral information (spectroscopic imaging) provides added value. Specific methods have been introduced that allow reaching below 100 μm resolution for the most challenging solid components. Contrast in the images or localization of the spectra using the additional spectroscopic, electrochemical and time dimensions still has its best days ahead.

16.9 References

1. Harks PPRML, Mulder FM, Notten PHL. In situ methods for Li-ion battery research: A review of recent developments. *Journal of Power Sources*. 2015;288:92–105.
2. Grey CP, Tarascon JM. Sustainability and in situ monitoring in battery development. *Nature Materials*. 2017;16(1):45–56.
3. Liu D, Shadik Z, Lin R, Qian K, Li H, Li K, et al. Review of Recent Development of In Situ/Operando Characterization Techniques for Lithium Battery Research. *Advanced Materials*. 2019;31(28):1806620.
4. Köckenberger W, Granwehr J. MR Microscopy. In: Lindon JC, editor. *Encyclopedia of Spectroscopy and Spectrometry (Second Edition)*. Oxford: Academic Press; 2010. p. 1654–62.
5. Pecher O, Carretero-González J, Griffith KJ, Grey CP. Materials' Methods: NMR in Battery Research. *Chem Mater*. 2017;29(1):213–42.
6. Borzutzki K, Brunklaus G. Chapter Three - Magnetic Resonance Imaging Studies of the Spatial Distribution of Charge Carriers. In: *Annual Reports on NMR Spectroscopy*. Academic Press; 2017. p. 115–41.
7. Vyalikh A, Köhler T, Zakharchenko T, Itkis DM, Krajnc A, Mali G. Magnetic resonance spectroscopy approaches for electrochemical research. *Physical Sciences Reviews*. 2018;3(10).
8. Mohammadi M, Jerschow A. In situ and operando magnetic resonance imaging of electrochemical cells: A perspective. *Journal of Magnetic Resonance*. 2019;308:106600.
9. Krachkovskiy S, Trudeau ML, Zaghbi K. Application of Magnetic Resonance Techniques to the In Situ Characterization of Li-Ion Batteries: A Review. *Materials*. 2020;13(7):1694.
10. Liu X, Liang Z, Xiang Y, Lin M, Li Q, Liu Z, et al. Solid-State NMR and MRI Spectroscopy for Li/Na Batteries: Materials, Interface, and In Situ Characterization. *Advanced Materials*. 2021;2005878.
11. Wakihara M, Yamamoto O. *Lithium Ion Batteries: Fundamentals and Performance*. Wiley-VCH; 1998. 261 p.
12. Conway E B. *Electrochemical Supercapacitors*. New York: Springer; 1999. 698 p.
13. Moseley PT, Garche J. *Electrochemical Energy Storage for Renewable Sources and Grid Balancing*. Elsevier; 2014.
14. Beard KW. *Linden's Handbook of Batteries*. 5th ed. McGraw-Hill Education: New York; 2019.

15. Tarascon J-M, Armand M. Issues and challenges facing rechargeable lithium batteries. *Nature*. 2001;414(6861):359–67.
16. Armand M, Tarascon J-M. Building better batteries. *Nature*. 2008;451(7179):652–7.
17. Choi JU, Voronina N, Sun Y-K, Myung S-T. Recent Progress and Perspective of Advanced High-Energy Co-Less Ni-Rich Cathodes for Li-Ion Batteries: Yesterday, Today, and Tomorrow. *Advanced Energy Materials*. 2020;10(42):2002027.
18. Asenbauer J, Eisenmann T, Kuenzel M, Kazzazi A, Chen Z, Bresser D. The success story of graphite as a lithium-ion anode material – fundamentals, remaining challenges, and recent developments including silicon (oxide) composites. *Sustainable Energy & Fuels*. 2020;4(11):5387–416.
19. Li P, Kim H, Myung S-T, Sun Y-K. Diverting Exploration of Silicon Anode into Practical Way: A Review Focused on Silicon-Graphite Composite for Lithium Ion Batteries. *Energy Storage Materials*. 2021;35:550–76.
20. Armand M, Axmann P, Bresser D, Copley M, Edström K, Ekberg C, et al. Lithium-ion batteries – Current state of the art and anticipated developments. *Journal of Power Sources*. 2020;479:228708.
21. Grey CP, Hall DS. Prospects for lithium-ion batteries and beyond—a 2030 vision. *Nature Communications*. 2020;11(1):6279.
22. Zhang H, Li C, Eshetu GG, Laruelle S, Grugeon S, Zaghbi K, et al. From Solid-Solution Electrodes and the Rocking-Chair Concept to Today’s Batteries. *Angewandte Chemie International Edition*. 2020;59(2):534–8.
23. Randau S, Weber DA, Kötz O, Koerver R, Braun P, Weber A, et al. Benchmarking the performance of all-solid-state lithium batteries. *Nature Energy*. 2020;5(3):259–70.
24. Tian Y, Zeng G, Rutt A, Shi T, Kim H, Wang J, et al. Promises and Challenges of Next-Generation “Beyond Li-ion” Batteries for Electric Vehicles and Grid Decarbonization. *Chem Rev*. 2021;121(3):1623–69.
25. Hasa I, Mariyappan S, Saurel D, Adelhelm P, Kozlov AY, Masquelier C, et al. Challenges of today for Na-based batteries of the future: From materials to cell metrics. *Journal of Power Sources*. 2021;482:228872.
26. Shao H, Wu Y-C, Lin Z, Taberna P-L, Simon P. Nanoporous carbon for electrochemical capacitive energy storage. *Chemical Society Reviews*. 2020;49(10):3005–39.
27. Slesinski A, Fic K, Frackowiak E. Chapter Six - New Trends in Electrochemical Capacitors. In: van Eldik R, Macyk W, editors. *Advances in Inorganic Chemistry*. Academic Press; 2018. p. 247–86. (Materials for Sustainable Energy; vol. 72).

28. Lin Z, Goikolea E, Balducci A, Naoi K, Taberna PL, Salanne M, et al. Materials for supercapacitors: When Li-ion battery power is not enough. *Materials Today*. 2018;21(4):419–36.
29. Ding J, Hu W, Paek E, Mitlin D. Review of Hybrid Ion Capacitors: From Aqueous to Lithium to Sodium. *Chem Rev*. 2018;118(14):6457–98.
30. Simon P, Gogotsi Y. Perspectives for electrochemical capacitors and related devices. *Nature Materials*. 2020;19(11):1151–63.
31. Yang X, Rogach AL. Electrochemical Techniques in Battery Research: A Tutorial for Nonelectrochemists. *Advanced Energy Materials*. 2019;9(25):1900747.
32. Dugas R, Forero-Saboya JD, Ponrouch A. Methods and Protocols for Reliable Electrochemical Testing in Post-Li Batteries (Na, K, Mg, and Ca). *Chem Mater*. 2019;31(21):8613–28.
33. Bard Ilen J, Faulkner L R. *Electrochemical Methods: Fundamentals and Applications*. 2nd edition. New York: Wiley; 2001.
34. Collins English Dictionary. In HarperCollins Publishers;
35. Callaghan PT. *Principles of Nuclear Magnetic Resonance Microscopy*. Oxford University Press; 2003.
36. Keeler J. *Understanding NMR Spectroscopy, 2nd Edition* | Wiley. 2010. 526 p.
37. Trease NM, Zhou L, Chang HJ, Zhu BY, Grey CP. In situ NMR of lithium ion batteries: Bulk susceptibility effects and practical considerations. *Solid State Nuclear Magnetic Resonance*. 2012;42:62–70.
38. Zhou L, Leskes M, Ilott AJ, Trease NM, Grey CP. Paramagnetic electrodes and bulk magnetic susceptibility effects in the in situ NMR studies of batteries: Application to $\text{Li}_{1.08}\text{Mn}_{1.92}\text{O}_4$ spinels. *Journal of Magnetic Resonance*. 2013;234:44–57.
39. Salager E, Sarou-Kanian V, Sathiya M, Tang M, Leriche J-B, Melin P, et al. Solid-State NMR of the Family of Positive Electrode Materials $\text{Li}_2\text{Ru}_{1-y}\text{Sn}_y\text{O}_3$ for Lithium-Ion Batteries. *Chem Mater*. 2014;26(24):7009–19.
40. Gerald II RE, Sanchez J, Johnson CS, Klingler RJ, Rathke JW. In situ nuclear magnetic resonance investigations of lithium ions in carbon electrode materials using a novel detector. *Journal of Physics: Condensed Matter*. 2001;13(36):8269.
41. Ilott AJ, Mohammadi M, Schauerman CM, Ganter MJ, Jerschow A. Rechargeable lithium-ion cell state of charge and defect detection by in-situ inside-out magnetic resonance imaging. *Nature Communications*. 2018;9(1):1776.
42. Romanenko K, Jerschow A. Distortion-free inside-out imaging for rapid diagnostics of rechargeable Li-ion cells. *PNAS*. 2019;116(38):18783–9.

43. Mohammadi M, Silletta EV, Ilott AJ, Jerschow A. Diagnosing Current Distributions in Batteries with Magnetic Resonance Imaging. *Journal of Magnetic Resonance*. 2019;106601.
44. Benders S, Mohammadi M, Klug CA, Jerschow A. Nuclear magnetic resonance spectroscopy of rechargeable pouch cell batteries: beating the skin depth by excitation and detection via the casing. *Scientific Reports*. 2020;10(1):13781.
45. Letellier M, Chevallier F, Clinard C, Frackowiak E, Rouzaud J-N, Béguin F, et al. The first in situ ⁷Li nuclear magnetic resonance study of lithium insertion in hard-carbon anode materials for Li-ion batteries. *The Journal of Chemical Physics*. 2003;118(13):6038.
46. Serša I, Mikac U. A study of MR signal reception from a model for a battery cell. *Journal of Magnetic Resonance*. 2018;294:7–15.
47. Krachkovskiy SA, Bazak JD, Werhun P, Balcom BJ, Halalay IC, Goward GR. Visualization of Steady-State Ionic Concentration Profiles Formed in Electrolytes during Li-Ion Battery Operation and Determination of Mass-Transport Properties by in Situ Magnetic Resonance Imaging. *J Am Chem Soc*. 2016;138(25):7992–9.
48. Bazak JD, Krachkovskiy SA, Goward GR. Multi-Temperature in Situ Magnetic Resonance Imaging of Polarization and Salt Precipitation in Lithium-Ion Battery Electrolytes. *J Phys Chem C*. 2017;121(38):20704–13.
49. Bazak JD, Allen JP, Krachkovskiy SA, Goward GR. Mapping of Lithium-Ion Battery Electrolyte Transport Properties and Limiting Currents with In Situ MRI. *J Electrochem Soc*. 2020;167(14):140518.
50. Letellier M, Chevallier F, Morcrette M. In situ ⁷Li nuclear magnetic resonance observation of the electrochemical intercalation of lithium in graphite; 1st cycle. *Carbon*. 2007;45(5):1025–34.
51. Pecher O, Carretero-González J, Griffith KJ, Grey CP. *Materials' Methods: NMR in Battery Research*. Chem Mater. 2016;
52. Tang JA, Dugar S, Zhong G, Dalal NS, Zheng JP, Yang Y, et al. Non-Destructive Monitoring of Charge-Discharge Cycles on Lithium Ion Batteries using ⁷Li Stray-Field Imaging. *Sci Rep*. 2013;3.
53. Tarascon J-M, Gozdz AS, Schmutz C, Shokoohi F, Warren PC. Performance of Bellcore's plastic rechargeable Li-ion batteries. *Solid State Ionics*. 1996;86:49–54.
54. Chevallier F, Letellier M, Morcrette M, Tarascon J-M, Frackowiak E, Rouzaud J-N, et al. In Situ ⁷Li-Nuclear Magnetic Resonance Observation of Reversible Lithium Insertion into Disordered Carbons. *Electrochemical and Solid-State Letters*. 2003;6(11):A225.
55. Chandrashekar S, Trease NM, Chang HJ, Du L-S, Grey CP, Jerschow A. ⁷Li MRI of Li batteries reveals location of microstructural lithium. *Nature Materials*. 2012;11(4):311–5.

56. Ilott AJ, Trease NM, Grey CP, Jerschow A. Multinuclear in situ magnetic resonance imaging of electrochemical double-layer capacitors. *Nat Commun.* 2014;5.
57. Poli F, Kshetrimayum JS, Monconduit L, Letellier M. New cell design for in-situ NMR studies of lithium-ion batteries. *Electrochemistry Communications.* 2011;13(12):1293–5.
58. Tang JA, Zhong G, Dugar S, Kitchen JA, Yang Y, Fu R. Solid-state STRAFI NMR probe for material imaging of quadrupolar nuclei. *Journal of Magnetic Resonance.* 2012;225:93–101.
59. Aguilera AR, MacMillan B, Krachkovskiy S, Sanders KJ, Alkhayri F, Adam Dyker C, et al. A parallel-plate RF probe and battery cartridge for ⁷Li ion battery studies. *Journal of Magnetic Resonance.* 2021;325:106943.
60. Freytag AI, Pauric AD, Krachkovskiy SA, Goward GR. In Situ Magic-Angle Spinning ⁷Li NMR Analysis of a Full Electrochemical Lithium-Ion Battery Using a Jelly Roll Cell Design. *J Am Chem Soc.* 2019;141(35):13758–61.
61. Freytag AI, Pauric AD, Jiang M, Goward GR. ⁷Li and ²⁹Si NMR Enabled by High-Density Cellulose-Based Electrodes in the Lithiation Process in Silicon and Silicon Monoxide Anodes. *J Phys Chem C.* 2019;123(18):11362–8.
62. Yon M, Sarou-Kanian V, Scheler U, Bouler J-M, Bujoli B, Massiot D, et al. Solid-state ³¹P and ¹H chemical MR micro-imaging of hard tissues and biomaterials with magic angle spinning at very high magnetic field. *Scientific Reports.* 2017;7(1):8224.
63. Romanenko K, Forsyth M, O’Dell LA. New opportunities for quantitative and time efficient 3D MRI of liquid and solid electrochemical cell components: Sectoral Fast Spin Echo and SPRITE. *Journal of Magnetic Resonance.* 2014;248:96–104.
64. Chien P-H, Griffith KJ, Liu H, Gan Z, Hu Y-Y. Recent Advances in Solid-State Nuclear Magnetic Resonance Techniques for Materials Research. *Annu Rev Mater Res.* 2020;50(1):493–520.
65. Bray JM, Doswell CL, Pavlovskaya GE, Chen L, Kishore B, Au H, et al. Operando visualisation of battery chemistry in a sodium-ion battery by ²³Na magnetic resonance imaging. *Nature Communications.* 2020;11(1):2083.
66. Krachkovskiy SA, Pauric AD, Halalay IC, Goward GR. Slice-Selective NMR Diffusion Measurements: A Robust and Reliable Tool for In Situ Characterization of Ion-Transport Properties in Lithium-Ion Battery Electrolytes. *J Phys Chem Lett.* 2013;4(22):3940–4.
67. Balbierer R, Seegert P, Herberger S, Wetzl T, Nirschl H, Guthausen G. Investigation of Transverse Relaxation Rate Distribution via Magnetic Resonance Imaging: Impact of Electrode Formation. *Energy Technology.* 2021;9:2000579.

68. Maudsley AA, Hilal SK, Perman WH, Simon HE. Spatially resolved high resolution spectroscopy by “four-dimensional” NMR. *Journal of Magnetic Resonance* (1969). 1983;51(1):147–52.
69. Ilott AJ, Chandrashekar S, Klöckner A, Chang HJ, Trease NM, Grey CP, et al. Visualizing skin effects in conductors with MRI: Li MRI experiments and calculations. *Journal of Magnetic Resonance*. 2014;245:143–9.
70. Bhattacharyya R, Key B, Chen H, Best AS, Hollenkamp AF, Grey CP. In situ NMR observation of the formation of metallic lithium microstructures in lithium batteries. *Nat Mater*. 2010;9(6):504–10.
71. Chang HJ, Ilott AJ, Trease NM, Mohammadi M, Jerschow A, Grey CP. Correlating Microstructural Lithium Metal Growth with Electrolyte Salt Depletion in Lithium Batteries Using ⁷Li MRI. *J Am Chem Soc*. 2015;137(48):15209–16.
72. Bayley PM, Trease NM, Grey CP. Insights into Electrochemical Sodium Metal Deposition as Probed with in Situ ²³Na NMR. *J Am Chem Soc*. 2016;138(6):1955–61.
73. Xiang Y, Zheng G, Liang Z, Jin Y, Liu X, Chen S, et al. Visualizing the growth process of sodium microstructures in sodium batteries by in-situ ²³Na MRI and NMR spectroscopy. *Nature Nanotechnology*. 2020;15(10):883–90.
74. Rees GJ, Jolly DS, Ning Z, Marrow TJ, Pavlovskaya GE, Bruce PG. Imaging Sodium Dendrite Growth in All-Solid-State Sodium Batteries Using ²³Na T₂-Weighted Magnetic Resonance Imaging. *Angewandte Chemie*. 2021;133(4):2138–43.
75. Marbella LE, Zekoll S, Kasemchainan J, Emge SP, Bruce PG, Grey CP. ⁷Li NMR Chemical Shift Imaging To Detect Microstructural Growth of Lithium in All-Solid-State Batteries. *Chem Mater*. 2019;
76. Pell AJ, Pintacuda G. Broadband solid-state MAS NMR of paramagnetic systems. *Progress in Nuclear Magnetic Resonance Spectroscopy*. 2015;84–85:33–72.
77. Tang M, Sarou-Kanian V, Melin P, Leriche J-B, Ménétrier M, Tarascon J-M, et al. Following lithiation fronts in paramagnetic electrodes with in situ magnetic resonance spectroscopic imaging. *Nat Commun*. 2016;7:13284.
78. Ordidge RJ, Connelly A, Lohman JAB. Image-selected in Vivo spectroscopy (ISIS). A new technique for spatially selective nmr spectroscopy. *Journal of Magnetic Resonance* (1969). 1986;66(2):283–94.
79. Maricq MM, Waugh JS. NMR in rotating solids. *J Chem Phys*. 1979;70(7):3300–16.
80. Wandt J, Marino C, Gasteiger HA, Jakes P, Eichel R-A, Granwehr J. Operando electron paramagnetic resonance spectroscopy – formation of mossy lithium on lithium anodes during charge–discharge cycling. *Energy Environ Sci*. 2015;8(4):1358–67.

81. Sathiya M, Leriche J-B, Salager E, Gourier D, Tarascon J-M, Vezin H. Electron paramagnetic resonance imaging for real-time monitoring of Li-ion batteries. *Nat Commun.* 2015;6.
82. Niemöller A, Jakes P, Eichel R-A, Granwehr J. EPR Imaging of Metallic Lithium and its Application to Dendrite Localisation in Battery Separators. *Sci Rep.* 2018;8(1):1–7.
83. Dutoit C-E, Tang M, Gourier D, Tarascon J-M, Vezin H, Salager E. Monitoring metallic sub-micrometric lithium structures in Li-ion batteries by in situ electron paramagnetic resonance correlated spectroscopy and imaging. *Nature Communications.* 2021;12(1):1410.